Author Manuscript

Author Manuscript

Author Manuscript

Author Manuscript

HHS Public Access

Author manuscript

Nat Immunol. Author manuscript; available in PMC 2016 September 28.

Published in final edited form as:

Nat Immunol. 2016 May ; 17(5): 495–504. doi:10.1038/ni.3409.

DNA polymerase-α regulates type I interferon activation through cytosolic RNA:DNA synthesis

Petro Starokadomskyy[1], **Terry Gemelli**[2], **Jonathan J. Rios**[2,3,4], **Chao Xing**[2,5], **Richard C. Wang**[6], **Haiying Li**[1], **Vladislav Pokatayev**[1], **Igor Dozmorov**[7], **Shaheen Khan**[7], **Naoteru Miyata**[1], **Guadalupe Fraile**[8], **Prithvi Raj**[7], **Zhe Xu**[9], **Zigang Xu**[9], **Lin Ma**[9], **Zhimiao Lin**[10], **Huijun Wang**[10,11,12], **Yong Yang**[10,11], **Dan Ben-Amitai**[13,14], **Naama Orenstein**[15], **Huda Mussaffi**[14,16], **Eulalia Baselga**[17], **Gianluca Tadini**[18,19], **Eyal Grunebaum**[20,21], **Adrijan Sarajlija**[22,23], **Konrad Krzewski**[24], **Edward K. Wakeland**[7], **Nan Yan**[1,25], **Maria Teresa de la Morena**[1,4,26], **Andrew R. Zinn**[1,2,*,†], and **Ezra Burstein**[1,27,*,†]

[1]Department of Internal Medicine, UT Southwestern Medical Center, Dallas, TX, USA

[2]Eugene McDermott Center for Human Growth & Development, UT Southwestern Medical Center, Dallas, TX, USA

[3]Sarah M. and Charles E. Seay Center for Musculoskeletal Research, Texas Scottish Rite Hospital for Children, Dallas, TX, USA

[4]Department of Pediatrics, UT Southwestern Medical Center, Dallas, TX, USA

[5]Department of Clinical Sciences, UT Southwestern Medical Center, Dallas, TX, USA

[6]Department of Dermatology, UT Southwestern Medical Center, Dallas, TX, USA

[7]Department of Immunology, UT Southwestern Medical Center, Dallas, TX, USA

[8]Department of Internal Medicine, Ramón y Cajal University Hospital, Madrid, Spain

[9]Department of Dermatology, Beijing Children's Hospital, Capital Medical University, Beijing, China

[10]Department of Dermatology, Peking University First Hospital, Beijing, China

[11]Peking-Tsinghua Center for Life Sciences, Beijing, China

Users may view, print, copy, and download text and data-mine the content in such documents, for the purposes of academic research, subject always to the full Conditions of use: http://www.nature.com/authors/editorial_policies/license.html#terms

[*]Correspondence to: ; Email: Ezra.Burstein@UTSouthwestern.edu; ; Email: Andrew.Zinn@UTSouthwestern.edu
[†]These authors contributed equally to this work.

ACCESSION CODES.

The primary RNA-seq data is archived in NCBI (accession number GSE72589).

AUTHOR CONTRIBUTIONS

A.R.Z. oversaw human genetic and splicing studies. Ez.B. oversaw cellular and biochemical studies. P.S. performed most of the cellular and biochemical experiments. H.L., N.M., S.K., P.R., K.K. did some biochemical analysis, T.G. analyzed human DNA samples and performed splicing studies. J.J.R. and C.X. analyzed WGS data. R.C.W. obtained skin biopsies and assisted with hTERT immortalization of fibroblasts. I.D. analyzed RNA Seq data. V.P. and N.Y. assisted with experiments using knockout MEF cell lines. E.K.W. assisted with analysis of cytoplasmic nucleic acids. M.T.M. performed clinical immunologic studies. G.F., Zh.X., Zi.H., L.M., Z.L., H.W., Y.Y., D.B.-A., N.O., H.M., Eu.B., G.T., E.G., and A.S. contributed subjects. Ez.B., A.R.Z., and P.S. wrote the manuscript.

COMPETING FINANCIAL INTERESTS

The authors declare no competing financial interests.

Author Manuscript Author Manuscript Author Manuscript Author Manuscript

[12]Academy for Advanced Interdisciplinary Studies, Peking University, Beijing, China

[13]Unit of Pediatric Dermatology, Schneider Children's Medical Center of Israel, Petach Tikva, Israel

[14]Sackler Faculty of Medicine, Tel Aviv University, Tel Aviv, Israel

[15]Genetics Unit, Schneider Children's Medical Center of Israel, Petach Tikva, Israel

[16]Pulmonology Institute, Schneider Children's Medical Center, Petach Tikva, Israel

[17]Department of Dermatology, Hospital de la Santa Creu i Sant Pau, Barcelona, Spain

[18]Pediatric Dermatology Unit and Pediatric Highly Intensive Care Unit, Department of Pathophysiology and Transplantation, University of Milan, Italy

[19]IRCCS Ca' Granda Ospedale Maggiore Policlinico, Milan, Italy

[20]Developmental & Stem Cell Biology Program, Hospital for Sick Children, Toronto, Ontario, Canada

[21]Division of Immunology and Allergy, Hospital for Sick Children, University of Toronto, Toronto, Ontario, Canada

[22]Mother and Child Health Care Institute of Serbia, Belgrade, Serbia

[23]School of Medicine, University of Belgrade, Belgrade, Serbia

[24]Laboratory of Immunogenetics, Receptor Cell Biology Section, NIAID / NIH, Rockville, MD, USA

[25]Department of Microbiology, UT Southwestern Medical Center, Dallas, TX, USA

[26]Children's Health, Dallas, TX, USA

[27]Department of Molecular Biology, UT Southwestern Medical Center, Dallas, TX, USA

Abstract

Aberrant nucleic acids generated during viral replication are the main trigger for antiviral immunity, and mutations disrupting nucleic acid metabolism can lead to autoinflammatory disorders. Here we investigated the etiology of X-linked reticulate pigmentary disorder (XLPDR), a primary immunodeficiency with autoinflammatory features. We discovered that XLPDR is caused by an intronic mutation that disrupts expression of *POLA1*, the gene encoding the catalytic subunit of DNA polymerase-α. Unexpectedly, *POLA1* deficiency results in increased type I interferon production. This enzyme is necessary for RNA:DNA primer synthesis during DNA replication and strikingly, POLA1 is also required for the synthesis of cytosolic RNA:DNA, which directly modulates interferon activation. Altogether, this work identified POLA1 as a critical regulator of the type I interferon response.

Innate immunity relies on the ability of the host to detect unique molecular patterns displayed by potential pathogens. Viruses and their distinctive replication cycles can generate a variety of aberrant nucleic acids that activate innate immune sensors, resulting in type I interferon production. Mutations affecting genes involved in these sensing mechanisms can lead to immunodeficiency in humans[1–3]. In addition, autoinflammatory

Author Manuscript Author Manuscript Author Manuscript Author Manuscript

syndromes characterized by spontaneous hyperactivation of the type I interferon pathway have been linked to mutations in various genes involved in nucleic acid metabolism or signaling. The most prominent condition in this category is Aicardi-Goutières syndrome (AGS), a rare genetic disorder affecting the brain, skin and other organs[4–6]. About half of AGS cases are due to mutations in any of the three subunits of the RNase H2 complex[7], a nuclease with RNase activity directed at RNA:DNA hybrids that is required for removal of misincorporated ribonucleotides or RNA primers generated during DNA replication[8]. In addition, studies of autoimmune disorders have highlighted that critical aspects of anti-viral signaling pathways in humans can be involved in the inherited susceptibility to systemic lupus erythematosus[9].

The study of defined syndromes of altered immune function can lead to powerful insights into gene function and the specific organization of immune responses in humans. With this goal in mind, we examined the genetic etiology of X-linked reticulate pigmentary disorder (XLPDR, MIM 301220), a rare entity characterized by both recurrent infections and sterile inflammation in various organs. To date, seven families and 14 affected individuals have been reported[10–18]. The disease typically manifests in the first few months of life, when patients usually develop recurrent pneumonias, bronchiectasis, chronic diarrhea and failure to thrive. Diffuse skin hyperpigmentation with a distinctive reticulate pattern is universally evident by early childhood, and this is later followed in many patients by hypohidrosis, corneal inflammation and scarring, enterocolitis resembling inflammatory bowel disease, and recurrent urethral strictures. Some of these features resemble the phenotypes associated with other mutations that affect immune function, particularly mutations in *IKBKG* (also known as NEMO), which can result in similar pigmentary changes and hypohidrosis[19]. Males with XLPDR also have a characteristic facies with frontally upswept hair and flared eyebrows. Female carriers are only known to have restricted pigmentary changes along Blaschko's lines.

Our report demonstrates that XLPDR is due to a unique hypomorphic mutation of the *POLA1* gene, encoding the catalytic subunit of DNA polymerase-α, an essential component of the DNA replication machinery. Furthermore, our results revealed a previously unrecognized role for this replicative polymerase as a modulator of interferon activation through the generation of cytosolic RNA:DNA hybrids.

RESULTS

XLPDR is caused by an intronic mutation in *POLA1*

Prior linkage analyses had mapped the *XLPDR* locus to a 4.9 Mb interval of the X chromosome[20]. However, Sanger and exome capture sequencing failed to identify any causal mutation. For the genetic analysis performed here, we included five of the seven known XLPDR families, as well as seven new families not previously reported (Fig. 1). The additional probands all displayed characteristic pigmentary changes of XLPDR, and most had the distinctive facies (Supplementary Fig. 1a). Skin biopsies from two new probands demonstrated the presence of melanophages and amyloid-like material in the upper dermis, as has been previously reported in XLPDR[10] (Supplementary Fig. 1b).

Author Manuscript Author Manuscript Author Manuscript Author Manuscript

Given the failure of prior sequencing efforts to identify a mutation in coding exons or flanking splice sites within the linkage interval, we performed whole genome sequencing (WGS) of four unrelated probands from Canada, Australia, Italy, and Waco, Texas (Fig. 1, red arrows). Within the previously identified linkage interval, we investigated both nonsynonymous protein-coding changes and non-coding variants predicted to affect mRNA splicing, searching for variants that targeted the same gene in all four probands. Due to the rarity and high penetrance of the disease, variants were excluded if present with minor allele frequency >1% among HapMap samples or the 1000 Genomes Project. Additional variants were excluded if they were present in WGS data from 18 males known not to have XLPDR whose genomes were sequenced using the same WGS method[21]. No gene in the linkage interval harbored rare nonsynonymous variants in all four patients, in agreement with prior exome sequencing efforts. However, all four probands shared the same rare intronic variant, chrX:24744696 (hg19), predicted to alter splicing of *POLA1*, a gene in the XLPDR linkage region (NM_016937.3:c.1375–354A>G). *POLA1* encodes the catalytic subunit of DNA polymerase-α, a DNA-directed DNA polymerase that in vertebrates exists in a stable complex with Primase. The Polα-Primase complex synthesizes RNA:DNA primers which initiate Okazaki fragment synthesis, and is therefore essential for DNA replication and cell proliferation[22–25].

As expected for a disease-causing mutation, the variant segregated with XLPDR or carrier status in five multiplex families tested (Fig. 1) and was absent from 1,133 genomes (452 male, 681 female) from an ethnically diverse cohort[26] (Supplementary Fig. 1c). Furthermore, DNA samples from other unrelated probands harbored the NM_016937.3:c.1375–354A>G variant (Fig. 1). Only two individuals with the diagnosis of XLPDR were negative for this variant: a previously reported child from Lebanon[17], and an atypical case from China who lacked the characteristic facial features of the syndrome (not shown here). Further analysis of these two individuals was not possible due to limited availability of DNA.

To further investigate *POLA1* as a candidate gene for XLPDR, we hypothesized that there would be a paucity of loss-of-function (LoF) variants identified in public resequencing cohorts. In agreement with this notion, the Exome Aggregation Consortium of 60,706 individuals analyzed by next-generation sequencing (ExAC database) reports two different predicted LoF splicing variants, each in only a single heterozygous female. However, closer inspection of the predicted effects of these variants suggests that they may not be true LoF (not shown here). To more robustly assess the population prevalence of potentially deleterious missense variants, the Residual Variation Intolerance Score (RVIS) for *POLA1* was ascertained[27]. The RVIS measures the departure from the average number of common functional mutations found in genes with a similar mutational burden at a genome-wide level. A negative score indicates that the gene has less common functional variation than predicted and most often reflects purifying selection. The RVIS for *POLA1* is −0.795, which corresponds to the 12th percentile for scores genome-wide. This indicates that *POLA1* is under significant purifying selection, as predicted for a gene with such essential biological functions.

Author Manuscript Author Manuscript Author Manuscript Author Manuscript

Given the recurrent nature of the variant among most cases with XLPDR, we performed kinship analysis[28] which indicated that the four individuals sequenced were no closer than 5th degree relatives. Around the shared *POLA1* intronic variant, two probands (P1 and P7) shared a segment of 140 kb estimated to be identical by descent using BEAGLE[29]. The other two probands (P4 and P5) did not share this segment, and at most shared 3.7 kb in this region. Thus, while two of the families showed evidence of a distant founder effect, other cases have clearly emerged independently. Furthermore, the South Dakota proband was found to carry a *de novo* POLA1 mutation (Fig. 1). Altogether, our genetic data indicated that a recurrent intronic mutation in *POLA1* is responsible for XLPDR.

The XLPDR mutation results in *POLA1* missplicing

Next, using dermal fibroblasts derived from three XLPDR probands and five control lines, we compared the expression levels of genes from the XLPDR linkage interval. Only *POLA1* was significantly underexpressed in XLPDR cells (Fig. 2a). Furthermore, POLA1 protein expression in fibroblasts was markedly reduced as well (Fig. 2b). Quantitation using Li-COR indicated that POLA1 protein levels in XLPDR fibroblasts were reduced to about 35% of that seen in wild-type cells, and this was closely matched by the reduction observed by qRT-PCR at the mRNA level (Fig. 2c). An analogous effect on mRNA and protein expression was noted in patient-derived lymphoblastoid cell lines (LCLs, Supplementary Fig. 1d,e,f). Despite having reduced POLA1 levels, mutant fibroblasts did not display altered proliferative capacity or changes in cell cycle distribution (Supplementary Fig. 2a,b). Similarly, mitogen-induced lymphocyte proliferation was unaffected in two probands from the Waco, Texas family (Supplementary Fig. 2c). Furthermore, POLA1 silencing by siRNA to a degree comparable to that seen in XLPDR did not lead to cell cycle arrest in HeLa cells with an integrated cell-cycle reporter system (Supplementary Fig. 2d). Thus, the reduction of *POLA1* expression in XLPDR did not appear to compromise cell replication, in agreement with the lack of a growth phenotype in most patients.

Next, we examined the mechanism by which the NM_016937.3:c.1375–354A>G variant disrupts *POLA1* gene expression. Bioinformatic analysis[30] predicted that the XLPDR mutation creates a splice donor site located 76 nucleotides downstream of a cryptic splice acceptor sequence present in the same intron, introducing a novel exon 13a into the *POLA1* transcript (Fig. 2d). Indeed, RT-PCR confirmed the presence of an aberrant *POLA1* transcript in mutant fibroblasts (Fig. 2e), which by sequencing included the predicted exon 13a. Transcript specific qRT-PCR (Fig. 2f) demonstrated a 65% reduction in wild-type mRNA levels in XLPDR fibroblasts, suggesting that a substantial proportion of missplicing occurs in these cells. The misspliced mRNA was much less abundant, suggesting that inclusion of exon 13a destabilizes the transcript. Meanwhile, in XLPDR-derived LCLs the aberrant transcript could be amplified only by RT-PCR primers specific to exon 13a (Supplementary Fig. 2e), suggesting that it is much less abundant in these cells compared to fibroblasts. To confirm that the intronic A>G mutation was solely responsible for aberrant splicing, we introduced *POLA1* intron 13 and its surrounding exons into an exon trapping plasmid system[31]. Intron 13 containing the XLPDR mutation led to two transcripts, and sequencing of the larger one confirmed the presence of exon 13a (Fig. 2g). Although the aberrant exon 13a introduces a frameshift mutation, immunoblotting showed no evidence of

Author Manuscript Author Manuscript Author Manuscript Author Manuscript

a truncated protein; only reduced expression of full-length POLA1 protein was observed (Supplementary Fig. 2f). Altogether, the data indicate that the XLPDR mutation creates a hypomorphic *POLA1* allele, ultimately reducing POLA1 protein expression. In addition, the data suggest that the magnitude of reduction of POLA1 expression may be subject to tissue-specific differences in missplicing.

POLA1 deficiency states activate type I interferon responses

To understand how *POLA1* might be linked to the XLPDR phenotype, we compared the transcriptome profiles of four control dermal fibroblasts lines against cells derived from two unrelated XLPDR patients (primary and telomerase-immortalized fibroblasts). Furthermore, we contrasted those findings to the effects of POLA1 silencing by siRNA in control fibroblasts (Fig. 3a,b). Compared to control fibroblasts, primary and immortalized XLPDR-derived cells displayed concordant alterations in gene expression for 177 genes, and nearly two-thirds of these changes (102 genes) were recapitulated by silencing of POLA1 in control fibroblasts (Fig. 3a, and Supplementary Table 1). Most of these changes represented increased gene expression in *POLA1* deficient cells (Fig. 3b). Ontology analysis indicated that these genes were primarily involved in the type I interferon signaling pathway, regulated by members of the IRF and NF-κB families of transcription factors (**Table**). Therefore, we analyzed the response of mutant cells to activation of IRF- or NF-κB-dependent gene expression, following poly(dA:dT) or tumor necrosis factor (TNF) stimulation, respectively. In both instances, *POLA1*-deficient cells primarily displayed more robust activation of genes that map to the IRF and NF-κB pathways (Fig. 3c,d, Supplementary Table 2). In the case of poly(dA:dT) treatment, 35% of the gene response was affected by *POLA1* deficiency, mostly resulting in greater gene expression (Fig. 3c, 137 of 387 genes). This included a number of genes such as *IFNA21*, several chemokines, NF-κB regulatory proteins, and multiple histone genes (Supplementary Table 1), which were minimally induced unless cells were *POLA1* deficient. Similar results were noted after TNF treatment, where nearly 40% of the responsive genes were affected by *POLA1* deficiency (Fig. 3d, 108 of 276 responsive genes). Mutant fibroblasts were not only hyper-responsive to poly(dA:dT) and TNF, but also to other forms of cytosolic dsDNA, cytosolic dsRNA, IL-1β, and Toll-like receptor (TLR) ligands (Supplementary Fig. 3a). Furthermore, these alterations were mimicked by siRNA-mediated silencing of POLA1 in wild-type fibroblasts and HeLa cells (Supplementary Fig. 3b). Collectively, these findings indicate that reduced POLA1 expression leads to constitutive enhancement of IRF and NF-κB dependent gene expression, including canonical interferon-stimulated genes (ISGs) and other pro-inflammatory factors.

XLPDR results in an interferon transcriptional signature

Given that activation of a similar interferon transcriptional signature has been noted in blood cells of patients with AGS[7], we examined next whether transcripts for several ISGs were affected in blood cells of XLPDR patients. Transcripts were measured in blood RNA from five patients (P1, P3, P7, P9, and P10) from four separate families (Fig. 1) and 14 healthy ‘travel’ control donors, including five heterozygous carriers. Each gene analyzed showed about 10-fold greater expression in XLPDR patients than in controls, which was statistically significant in every case (Fig. 3e). These results indicate that reduced *POLA1* expression

Author Manuscript Author Manuscript Author Manuscript Author Manuscript

leads to constitutive activation of IRF and NF-κB dependent genes, resulting in a strong type-I interferon response in XLPDR patients, similar to alterations noted in AGS[9].

The clinical phenotype of XLPDR is distinct from AGS

In view of the molecular similarities between XLPDR and AGS, we performed a more extensive analysis of the clinical phenotype of our patient cohort, directly contrasting it to known manifestations of AGS[6] (Supplementary Table 3). Similar to AGS, several patients reported a history of more severe manifestations during early infancy, resulting in failure to thrive (57.1%), which eventually improved spontaneously. However, there was little overlap with the core neurologic manifestations of AGS[6], with only 2 individuals having a history of developmental delay (14.3%). Digital vasculitis and/or necrosis (chilblains), which are common in AGS, were not reported in our patients. Rather, XLPDR was characterized by a unique combination of diffuse hyperpigmentation (100%), a characteristic facies (100%), recurrent lung infections (92.9%) and hypohidrosis (64.3%). Additionally, these patients experienced unique autoinflammatory phenomena affecting the gastrointestinal tract (64.3%), cornea (50%), and urinary tract (35.7%). Autoimmune manifestations were not reported and the patients did not have elevated ANA titers or evidence of any other autoantibodies (Supplementary Fig. 4a,b and Supplementary Table 4).

XLPDR patients display increased type-I IFN

Most XLPDR patients reported a history of recurrent bacterial infections involving the lung and upper respiratory tract, but other invasive infections (meningitis, osteomyelitis, skin abscesses) were not reported. The cultured organisms included *Streptococcus pneumoniae, Haemophilus influenza, Staphylococcus aureus, Streptococcus pyogenes,* and *Pseudomonas aeruginosa*. Two patients (14.3%) had histories of pulmonary mycobacterial infections (*Mycobaterium tuberculosis* and *Mycobacterium avium-intracellulare*), and two individuals also had candidiasis (Supplementary Table 3). In terms of functional analysis of the immune system, some patients displayed mild neutrophilia and lymphopenia, but morphologic features of white blood cells, including myeloid cell ultrastructure, were normal (Supplementary Fig. 4c). There were no changes in critical lymphoid sub-populations or oxidative burst capacity of neutrophils. Immunoglobulin concentration in serum was largely normal, except for either elevation or reduction in IgE levels of unclear significance. When tested, antibody responses to vaccination antigens were also normal (Supplementary Table 3).

To further investigate immune function in XLPDR, plasma concentrations of 38 cytokines were examined (Supplementary Table 5 and Fig. 3f). IFNα2 concentrations were significantly elevated in these patients (Fig. 3f), in agreement with the activated ISG signature noted in blood mRNA (Fig. 3e). Moreover, 8 additional factors were significantly elevated, including very dramatic elevations of IL-8 concentration. Conversely, two cytokines – IFN-γ and IL-17A – were significantly reduced compared to healthy controls. IFN-γ suppression has been reported in patients with *ISG15* mutations, who display features of AGS as well as increased susceptibility to mycobacterial infection[32, 33]. Similarly, defects in IL-17 signaling have been linked to pyogenic infections with *S. aureus* as well as chronic mucocutaneous candidiasis[34]. Altogether, the immunological phenotype of these patients is

Author Manuscript Author Manuscript Author Manuscript Author Manuscript

characterized by autoinflammatory manifestations, which are likely related to chronic type-I interferon production. In addition, these patients display suppressed IL-17A production – perhaps linked to their susceptibility to pyogenic infections–, and reduced IFN-γ production, which might be linked to mycobacterial infections.

POLA1 deficiency leads to TBK1 and IKK activation

Next, we examined whether signaling events that activate the IRF and NF-κB pathways are upregulated by *POLA1* deficiency. In the IRF pathway, activation of various sensors results in the phosphorylation of the TBK1 and IKKε kinases, which in turn then phosphorylate IRF family members, promoting their dimerization and nuclear translocation[35]. Fibroblasts from XLPDR patients displayed robust TBK1 phosphorylation, even at baseline conditions, far exceeding the signature noted in wild-type cells (Fig. 4a). Similarly, silencing of POLA1 in HeLa cells led to phosphorylation of both TBK1 and IKKε, which exceeded that achieved in control cells after stimulation with poly(dA:dT). This signature was accompanied by enhanced phosphorylation of IRF3 in nuclear fractions (Fig. 4b). In the NF-κB pathway, we found that XLPDR fibroblasts achieved similar degrees of IκB degradation and nuclear NF-κB (RelA) accumulation after TNF stimulation (Fig. 4c and Supplementary Fig. 5a,b). However, in both fibroblasts and HeLa cells, *POLA1* deficiency was associated with greater phosphorylation of RelA (Fig. 4c,d), which were also quantified using Li-COR (Supplementary Fig. 5c). This event is mediated by the IKK complex and can increase transcriptional induction[36]. In agreement with this finding, the phosphorylated and active forms of IKK1 and IKK2 were increased in patient fibroblasts as well as in HeLa cells after siRNA-mediated silencing of POLA1 (Fig. 4e). Thus, these data show that *POLA1* deficiency leads to activation of signaling cascades that converge on TBK1, IKKε and the IKK complex. Blockade of TBK1 using a specific kinase inhibitor was sufficient to reverse the increased ISG expression (Fig. 4f), indicating that the activation of this kinase in XLPDR cells is necessary for the activation of IRF and its downstream gene targets. Altogether, these data indicate that POLA1 deficiency results in augmented signals converging on key kinases that activate IRF and NF-κB.

POLA1 deficiency leads to reduced cytosolic RNA:DNA hybrids

To explain the constitutive activation of the IRF pathway in XLPDR, we examined whether increased amounts of cytosolic nucleic acids could be a possible trigger. To this end, we used antibodies with defined reactivities against specific nucleic acids to immunoprecipitate these molecules from cytosolic fractions and stained the recovered material with PicoGreen®, a double-stranded nucleic acid dye (Fig. 5a). Cytosolic dsDNA was mildly decreased in XLPDR fibroblasts, whereas cytosolic RNA:DNA was almost undetectable (Fig. 5b). The reduction in cytosolic RNA:DNA observed in XLPDR fibroblasts was also seen after silencing of POLA1 in HEK293T and HeLa cells (Fig. 5c and Supplementary Fig. 6a,b).

We then examined whether the defect in cytosolic RNA:DNA present in XLPDR fibroblasts could be rescued by re-expression of POLA1. Lentiviral transduction of POLA1 in these cells led to increased cytosolic RNA:DNA (Fig. 5d). This rescue was accompanied by dramatic reduction in phospho-TBK1 levels (Fig. 5e) and normalization of poly(dA:dT)-

Author Manuscript Author Manuscript Author Manuscript Author Manuscript

dependent *IFIT1* induction (Fig. 5f). Thus, POLA1 deficiency leads to decreased cytosolic RNA:DNA levels, which correlate directly with the XLPDR cellular phenotype.

POLA1 polymerase activity sustains cytosolic RNA:DNA levels

As mentioned previously, the role of the Polα-Primase complex during DNA replication is to synthesize an RNA:DNA primer on a DNA template strand[22], suggesting a possible direct link between POLA1 polymerase activity and the synthesis of cytosolic RNA:DNA. To test this notion, we first examined the subcellular localization of POLA1 and found that a substantial proportion of POLA1 localized to the cytosol, as determined by both immmunofluoresce staining and biochemical fractionation (Supplementary Fig. 7a,b). Moreover, cytosolic POLA1 colocalized with RNA:DNA with a speckled pattern (Supplementary Fig. 7c). Indeed, cytosolic POLA1 (and not other DNA binding proteins tested) co-immunoprecipitated with nucleic acids, as determined by PicoGreen® staining of beads (Fig. 6a). This material was sensitive to both DNase and RNase treatment (Fig. 6b), and after elution from POLA1, could in part be re-immunoprecipitated by the RNA:DNA antibody (Fig. 6c). The eluted nucleic acids could be resolved by on-chip capillary electrophoresis or by agarose gel electrophoresis and consisted predominantly of 40–100 bp fragments (Fig. 6d,e). Thus, cytosolic POLA1 associates with short nucleic acids, which at least in part include RNA:DNA.

Next, we evaluated whether the polymerase activity of POLA1 is involved in cytosolic RNA:DNA generation. Cytosolic RNA:DNA levels, which by immunoprecipitation and bead staining were reduced by POLA1 silencing, could be rescued by re-expression of wild-type POLA1; however, a polymerase-deficient form of POLA1 did not rescue cytosolic RNA:DNA levels, and in fact had a dominant negative effect (Fig. 6f, Supplementary Fig. 8). In aggregate, these studies indicate that POLA1, through its polymerase activity, is responsible for a significant proportion of the physiologic concentration of cytosolic RNA:DNA hybrids.

Cytosolic RNA:DNA downregulates antiviral gene expression

Next, we examined whether the generation of cytosolic RNA:DNA could be directly responsible for modulating IRF activation. First, we isolated cytosolic RNA:DNA through immunoprecipitation and nucleic acid purification; this material was then transfected into cells after POLA1 silencing. Cytosolic RNA:DNA transfection normalized the increased expression of IRF target genes resulting from POLA1 deficiency (Fig. 6g). Next, we tested whether synthetic nucleic acids can recapitulate the effects of native cytosolic RNA:DNA. We made synthetic RNA:DNA duplexes consisting of 30 bp of DNA annealed to an RNA:DNA strand (consisting of 10 RNA and 20 DNA bp), meant to mimic the RNA:DNA primer that is synthesized by the Polα-Primase complex during DNA replication. Transfection of this material indicated that RNA:DNA duplexes of this type can suppress the abnormal activation of IRF target genes observed as a result of *POLA1* deficiency (Fig. 6h). Thus, endogenous and synthetic RNA:DNA hybrids can directly rescue the effects of POLA1 deficiency – at least with respect to select ISG expression.

Author Manuscript Author Manuscript Author Manuscript Author Manuscript

Cytosolic RNA:DNA modulates nucleic acid sensor pathways

Finally, we examined whether the effects of cytosolic RNA:DNA hybrids can be mapped to a specific nucleic acid sensor pathway upstream of TBK1. To test this question, we used primary mouse embryo fibroblasts with defects in key genes involved in nucleic acid sensing: *Myd88*$^{-/-}$*Ticam1*$^{-/-}$ (Myd88 x TRIF double knockout), *Tmem173*$^{-/-}$ (Sting knockout), *Cgas*$^{-/-}$ (also known as *Mb21d1* and encoding cGAS), and *Mavs*$^{-/-}$. Using these cells, we found that *Cgas*$^{-/-}$ and *Mavs*$^{-/-}$ fibroblasts were particularly resistant to the effects of Pola1 siRNA (Fig. 7). Loss of other sensor pathways also partially rescued the phenotype associated with POLA1 deficiency. These findings suggest that cytosolic RNA:DNA preferentially regulates pathways upstream of MAVS and cGAS and may potentially have broader effects on other nucleic acid sensors.

DISCUSSION

This study demonstrates that XLPDR is caused by a recurrent intronic mutation resulting in missplicing and reduced *POLA1* expression. This mutation previously escaped detection because it lies deep within an intron, highlighting the utility of WGS for elucidating the genetic basis of rare diseases. That a unique *POLA1* mutation causes XLPDR is intriguing. The recurrent nature of the mutation might indicate that this genomic position is a mutational hotspot. When considering this possibility, it is important to note that this mutation might result in tissue-specific effects on missplicing and variable effects on *POLA1* expression. If this is the case, other mutations causing ubiquitous *POLA1* deficiency likely result in phenotypes such as AGS, a possibility that will require future investigation. Therefore, it is possible that phenotypic ascertainment and not mutational frequency might be responsible for the fact that we found only one mutation associated with XLPDR. The notion that the XLPDR mutation results in a gain-of-function effect cannot be completely excluded, but seems quite unlikely since we did not detect any aberrant protein but instead observed perfectly concordant cellular phenotypes of the XLPDR mutation and POLA1 siRNA silencing.

This study also provides a detailed characterization of this syndrome, including a careful evaluation of the immune phenotypes in these patients. As shown here, XLPDR has the molecular signature of an interferonopathy and is associated with suppressed IL-17A and IFN-γ, changes that are probably linked to the history of autoinflammation and recurrent infections. Interestingly, suppression of IL-17A has been previously linked to IRF activation[37]. While these molecular features are similar to those of AGS, most of the clinical features of XLPDR are quite distinct, including the paucity of neurologic involvement which is central to the presentation of most AGS cases. In addition, the development of hyperpigmentation, hypohidrosis, and facial features in XLPDR remain unexplained from a mechanistic standpoint. We anticipate that as additional cases are identified, new insights into the pathogenesis of this disorder will be gained. The role that POLA1 plays in cytosolic RNA:DNA synthesis was completely unexpected, based on our current knowledge of the Polα-Primase complex. We predict that this complex mediates the same biochemical steps in cytosolic nucleic acid biosynthesis as have been previously defined during DNA replication; as such, template DNA is the likely substrate for cytosolic RNA:DNA synthesis and the

Author Manuscript Author Manuscript Author Manuscript Author Manuscript

source for this DNA will need to be ascertained. This nonreplicative function for *POLA1* is in agreement with its abundant cytosolic localization in many cell types and its persistent expression in post-mitotic cells[38, 39].

Similarly, the finding that cytosolic RNA:DNA plays a role in preventing spontaneous activation of the IRF pathway was also quite unexpected. These data stand in contrast with prior reports that synthetic RNA:DNA duplexes can have stimulatory effects. It is therefore important to note key differences in our approach compared to prior studies[40]. First, to our knowledge, this is the first study to test the effect of native RNA:DNA extracted directly from the cytosol. This material captures the heterogeneity of chemistry and nucleotide length that is likely present *in vivo*, including possible hybrid duplexes (DNA annealed to RNA), or hybrid strands (ribonucleotides and deoxinucleotides linked together), or a combination of these. Thus, this experiment avoids the use of RNA:DNA chemistries of unclear physiologic relevance such as long synthetic palindromic RNA:DNA duplexes (> 1kb), which according to our analysis do not represent the predominant composition of cytosolic RNA:DNA. In addition, for studies with synthetic nucleotides, we used RNA:DNA consisting of a short duplex DNA strand annealed to a hybrid RNA:DNA strand, meant to recapitulate the product synthesized by Polα-Primase during DNA replication. In aggregate, our results suggest a mechanistic model where RNA:DNA hybrids synthesized by cytosolic POLA1 act to squelch the responses generated by stimulatory nucleic acids. One possible mechanism might be that cytosolic RNA:DNA could bind to nucleic acid sensors without triggering their activation, competing with their cognate ligands, and thus setting a higher threshold for signal generation. Based on the genetic evidence presented here, cytosolic RNA:DNA may in fact modulate multiple sensors. Finally, the fact that partial reduction of POLA1 expression alters immune regulation without blocking DNA replication suggests that DNA polymerase-α may provide a new target for therapeutic modulation of innate immunity.

ONLINE METHODS

Human studies

Genetic and immunological analyses of affected patients and family members were performed after obtaining informed consent. All the studies were reviewed and approved by the Institutional Review Board at UT Southwestern and collaborating institutions.

Genetic studies

Sequencing and variant detection were performed by Complete Genomics, resulting in >50-fold coverage in all four samples, which was sufficient to detect variants in >96% of the genome in all patients. We investigated both protein-coding and non-coding variants within the previously identified 4.9 Mb linkage interval. Variants were excluded if present with minor allele frequency (MAF) >1% among HapMap samples sequenced by Complete Genomics or among multiple subpopulations (AFR, SAS, EAS, EUR, AMR) of the 1000 Genomes Project. Additional high-quality variants in this interval were excluded if they were present in WGS data from 18 males known not to have XLPDR, whose genomes were sequenced using the same WGS method[21]. The resulting candidate variants in each patient

Author Manuscript Author Manuscript Author Manuscript Author Manuscript

were annotated for their potential effects on protein function (coding variants) and splicing (non-coding intronic variants). The latter analysis was performed using the Alamut software (Interactive Biosoftware), which integrates splicing prediction from multiple programs, including MaxEntScan, NNSPLICE and Human Splicing Finder. Kinship and ancestry analyses were performed using ERSA[28] and BEAGLE[29]. For genotyping of normal individuals in the Dallas Heart Study, we developed a specific 5' nucleotidase Taqman® allelic discrimination assay to genotype additional subjects for chrX:24744696 A/G using the Applied Biosystems HT7900 Real-Time PCR system and probes and reagents purchased from Life Technologies.

Cell culture and transfection

Human embryonic kidney (HEK) 293T cells and HeLa cells were obtained from ATCC; HeLa FUCCI was a kind gift from Dr. Lienhard Schmitz's laboratory. Both cell lines were cultured in DMEM supplemented with 10% FBS and L-glutamine. Knockout murine fibroblasts were harvested from mice with the indicated genotypes, as described by us in a previous study[41]. Patient-derived cell lines were obtained after IRB approval and informed consent. Lymphoblastoid cell lines (LCL) were generated by immortalization of peripheral lymphocytes with EBNA as previously described[42], and were cultured in RPMI 1640 (Cellgro, 10–040-CM) supplemented with 10% FBS. Primary human fibroblasts of XLPDR patients and relatives were obtained from skin punch biopsies. After 1 week in tissue culture, fibroblasts were immortalized by retroviral delivery of the human telomerase gene (a gift of Jerry Shay) followed by negative antibiotic selection for 2 weeks with puromycin (1 μg/mL). Both primary and immortalized fibroblasts were cultured in DMEM supplemented with 10% FBS. All cell lines used in this study were tested for Mycoplasma using a PCR-based method[43]; this testing was performed upon obtaining the cells and every 8–12 weeks to confirm that all experiments were performed in uninfected cells. For plasmid and siRNA transfection of HEK293T the standard calcium transfection was used[44]. For siRNA transfection in HeLa, HeLa FUCCI, and fibroblasts, the DharmaFECT transfection system (Dharmafect #4, T-2004–03, Dharmacon) was used according to the manufacturer's instructions. In certain experiments, TNF (1000 U/mL; Roche), IL1-β (1 μg/mL, Invivogen), poly(I:C) (250 μg/mL, Fisher), LPS (lipopolysaccharide from E. coli 0111:B4, 10 μg/mL; Invivogen), Pam3CSK4 (250 μg/mL, Invivogen) were applied to the growth media . Poly(dA:dT) (1 μg/mL, Invivogen), poly(I:C) (1 μg/mL, Fisher), HSV-60 (1 μg/mL, 60 bp oligonucleotide containing viral DNA motifs, Invivogen), ISD (1 μg/mL, interferon stimulatory DNA, Invivogen), and 5ppp-dsRNA (0.5 μg/mL, Invivogen) were transfected using standard calcium transcfection method for HEK293T, or using LyoVec (Invivogen) for HeLa cells and fibroblasts following the manufacturer's instructions.

Plasmids, lentiviral production and siRNA

pReceiver-Control, pReceiver-HA_3-POLA1wt, and pReceiver-HA_3-POLA1-G841A (encoding a point mutation that disables polymerase activity) were purchased from Genecopoeia. The lentiviral packaging plasmids pHCMV-VSV-G, pMDLg/pRRE, and pRSV-Rev were kindly provided by Dr. David Baltimore. Recombinant lentiviruses were generated by cotransfection of packaging plasmids in HEK293T, followed by viral particle harvest and target line infection, according to a standard procedure[45]. RNA duplexes used

Author Manuscript Author Manuscript Author Manuscript Author Manuscript

for siRNA were purchased from Sigma-Aldrich and included the following: control non-target siRNA (SIC002), human POLA1 #1 (SASI_Hs01_00138924), human POLA1 #2 (SASI_Hs01_00138925), and mouse Pola1 (SASI_Mm02_00314904).

RT-PCR

RNA was extracted using Trizol (Invitrogen) according to the manufacturer's instructions. RNA (5μg) was used for cDNA synthesis utilizing the Superscript III strand synthesis system (Invitrogen). For qualitative analysis of *POLA1* transcripts, the following primer sequences were utilized: primer A (exon 10, 5'-AAAGGGGCAGATGAGGAACAA-3'); primer X (exon 13a, 5'-TCTGACAGTGGTGATGAAAAG-3'); primer B (exon 15, 5'-ACAAG CGGTGGTGGACTGAC-3'). Quantitative real-time RT-PCR was performed using SYBR Green based detection (Invitrogen) and a Mastercycler (Eppendorf, Germany) as previously reported[46]. Experiments were performed using technical duplicates or triplicates, data were normalized to housekeeping genes and the relative abundance of transcripts was calculated by the comparative *ΔΔCt* method. All primers used for qRT-PCR are indicated in Supplementary Table 6.

Exon trapping analysis

A fragment of the *POLA1* gene containing exon 13–14 and flanking sequences was PCR amplified from control or XLPDR genomic DNA using high fidelity *Pfx* polymerase (Invitrogen) and cloned into pSpliceExpress (Addgene, Cambridge, MA). Plasmids were sequenced to confirm that no additional mutations were introduced during cloning. DNAs were transfected into HEK293 cells, and RNA extracted 48 hours later and RT-PCR amplified using primers from *POLA1* exon 13 (5'-ATGCTTTTGAGATACCTGAT-3') and pSpliceExpress rat insulin exon 2 (5'-GGCCTCCACCCAGCTCCAGTTGT-3'). Gel-purified products were Sanger-sequenced.

RNA-seq and gene expression data analysis

RNA was extracted using the RNeasy chromatography method (Qiagen), according to the manufacturer's instructions. RNA-seq libraries were prepared with the Illumina TruSeq RNA Sample Preparation kit (Illumina) according to the manufacturer's protocol. Libraries were validated on an Agilent Bioanalyzer 2100. The standard protocol from Illumina for the preparation of RNA-SEQ libraries from total RNA includes a step in which polyA mRNA selection results in the removal of the bulk rRNA from the sample, which results in the removal of background signal. Synthesis of first and second strand cDNA was followed by end repair and addition of "A" to the ends and ligations of the adapters for sample multiplexing. Enrichment of the samples was carried out by PCR. The amplified libraries were size selected and libraries were quantified by PicoGreen® assay (Life Technologies). We used TruSeqTM SR Cluster Kits v3 (Illumina Inc.; San Diego, CA) for cluster generation in an Illumina cBOT instrument following the manufacturer's protocol. Six indexed libraries were loaded into each lane of flow cells. Sequencing was performed on an Illumina HiSeq 2500 instrument (Illumina) by the manufacturer's protocol. Multiplexed five single-read runs were carried out with a total of 57 cycles per run (including 7 cycles for the index sequences). Custom programs were used to demuliplex individual samples using their

Author Manuscript Author Manuscript Author Manuscript Author Manuscript

unique index. Approximately 235 Million pass filter reads were achieved per lane. Each sample had close to 19.5 million reads.

We used CLC Genomics Workbench 7 for RNASEQ alignment and statistical analysis of the data. Human HG19 was used as reference sequence. The expression for the genes expressed in all samples was calculated. Methods for data normalization and analysis are based on the use of “internal standards” that that characterize some aspects of the system’s behavior, such as technical variability, as presented elsewhere[47]. The comparison of these methods with some other normalization and analysis procedures was previously reported[48]. Created initially for the analysis of microarray data, they were slightly modified to the needs of RNA-seq data analysis. The two-step normalization procedure and the Associative analysis functions were implemented in MatLab (Mathworks, MA). These algorithms are obtainable from an R package diffGeneAnalysis, available as a part of Bioconductor packages (http://www.bioconductor.org/packages/2.5/bioc/html/diffGeneAnalysis.html). Heatmaps were generated with the Spotfire Decision Site 9 (TIBCO, Palo Alto, CA) with gene subsets created from the list of significant genes. Functional analysis of identified genes was performed with Ingenuity Pathway Analysis (IPA; Ingenuity® Systems, Redwood City, CA, http://www.ingenuity.com).

Cell proliferation analyses

For DNA content analysis, ~1×10^6 cells were resuspended in PBS, and fixed in cold 70% ethanol for 30 min at 4°C. Fixed fibroblasts were washed twice with PBS and treated 15 min at RT with ribonuclease A (5 μg/mL, Qiagen), with subsequent staining with propidium iodide (500 ng/mL, Sigma-Aldrich). Cells were analyzed by flow cytometry using FACSCalibur (BD Biosciences) and the FlowJo software. FUCCI cells were similarly analyzed by FACS using the EGFP and DsRed indicator proteins. Mitogen stimulation of lymphocytes was performed by the Diagnostic Immunology Laboratory at Cincinnati Children’s Hospital as part of medical care due to the history of recurrent infections.

Immunofluorescence staining

Cells were growing in Nunc Lab-Tek Chamber slides (Thermo) for 48 hours. Cells were fixed in ice-cold 100% methanol for 15 minutes, and washed 3 times with PBS. Blocking buffer was applied (5% human serum, 1% glycerol, 0.1% BSA, 0.1% fish skin gelatin, 0.04% sodium azide, in PBS, pH 7.2). If required, selected samples were incubated with 0.25 μg/μL RNase A (Invitrogen) at 37°C for 30 minutes. Samples were incubated in a humidifier chamber overnight at 4°C with primary antibodies diluted in blocking buffer (POLA1, polyclonal, Santa Cruz, sc-5921, dilution 1:50; RNA:DNA, clone S9.6, Kerafast, ENH001, dilution 1:50; RelA, polyclonal, Santa Cruz, sc-372, dilution 1:500). Following 3 washes in PBS, cells were incubated with secondary Abs with the dilution 1:500 in blocking buffer (Alexa Fluor 568 donkey anti-rabbit, Alexa Fluor 594 chicken anti-mouse, Alexa 647 donkey anti-goat, from Jackson Immunoresearch) for 1 hr at room temperature in a humidifier chamber. After 4 washes in PBS and addition of Hoechst 33342 nuclear stain, coverslips were rinsed in water and affixed to slides with Slowfade Antifade reagent (Invitrogen). Images were obtained with an LSM-710 laser scanning confocal microscope with a 60×/1.4 Oil Plan-Aprochromat objective lens using ZEN software (Carl Zeiss).

Author Manuscript Author Manuscript Author Manuscript Author Manuscript

TBK1 inhibition

Mouse fibroblasts were transfected with siRNA targeting Pola1 or control sequence. After 48 hours, the cells were washed with PBS, and fresh media was applied containing 10 μM BX795 (Sigma) or vehicle (DMSO) as control. After 6 hours, the cells were washed with PBS, and RNA was extracted using Trizol (Sigma).

Plasma Cytokine Multiplex analysis

Blood samples from XLPDR patients and healthy controls were obtained in duplicates by local hospitals. EDTA-Plasma was separated from blood samples by centrifugation and stored at -80°C. Samples were analyzed with Human Cytokine/Chemokine Magnetic Bead Panel (Milliplex, HCYTMAG-60K-PX38, Millipore) on Luminex Magpix with the Luminex xPONENT software according to manufacturer's instructions. Data analysis was done using Milliplex Analyst.

ANA ELISA assay

ELISA was used to screen for presence of antinuclear antibodies (ANA) (Inova Diagnostics Inc., San Diego, CA). About 5 μL of human serum was used for each reaction in a dilution of 1:41. ANA ELISA detect antibodies to various nuclear antigens such as chromatin, Sm/RNP, SS-A, SS-B. Scl-70, centromere, PCNA, Jo-1 and ribosomal proteins. The assay was performed and results were interpreted as per manufacturer's instructions. The manufacturer's definition of positivity for ANA is greater than 20 units.

Autoantigen array

Autoantigen microarrays were manufactured, hybridizated and scanned as previously described[49]. Briefly, antigens were diluted to printing concentration in printing buffer (Whatman, Sanford, ME, USA) and transferred to 384-well plates. The antigens were printed in duplicate onto nitrocellulose-coated 16-pad FASTTM slides (Whatman, Sanford, ME, USA) by MicroGrid II 610 bio-robotics array printer (Genomic Solutions Inc., Ann Arbor, MI, USA). After printing, the slides were kept in a chamber with 70% humidity for 4 hours at room temperature, and stored at 4ºC. For hybridization, the slides were warmed up to room temperature for about 15 min, and then 60 μL of blocking buffer (Whatman, Sanford, ME, USA) was added to each array for 60 min. Serum samples were pretreated with DNAse-I (50 U/ml) for 30 min at room temperature in buffer containing 50 mM Tris-HCl, 75 mM KCl, 3 mM MgCl2, pH 8.3. The pretreated serum samples were diluted 1:50 in blocking buffer, and then added to each array for 1 hour. After that, each array was washed with 100 μL of washing buffer (Whatman, Sanford, ME, USA) three times for 5 min each, and then Cy3-conjugated anti-human IgG and Cy5-conjugated anti-human IgM (Jackson ImmunoResearch, West Grove, PA, USA) were applied at 1:1000 dilution to each array and incubated at room temperature for 1 hour. Genepix 4000B scanner with 532 nm and 635 nm wavelengths and Genepix Pro6.0 software were used for generate the Gene Pix Results (GPR) files. The net fluorescence intensities (nfi) were normalized by using anti-human IgG/IgM on each array. Heat maps were generated using Cluster and Treeview software (http://rana.bl.gov/EisenSoftware.htm).

Author Manuscript Author Manuscript Author Manuscript Author Manuscript

Whole blood RNA analysis

Blood samples from XLPDR patients and healthy controls were collected into PAXgene tubes (762165, PreAnalytix) in local hospitals in triplicates, stored at -80°C, and shipped on dry ice. mRNA was isolated following the manufacturer's instruction, and analyzed by qRT-PCR as described above.

Protein extraction, immunoblotting and immunoprecipitation

Cell lysate preparation, immunoprecipitation, denatured immunoprecipitation and immunoblotting were performed as previously described[46]. For Li-COR analysis, proteins were visualized using Odyssey Quantitative Fluorescent Imaging System (LI-COR Biosciences, Lincoln, NE). IR Dye 680 conjugated anti-mouse and anti-rabbit, and IR Dye 800 conjugated anti-goat, anti-rabbit and anti-mouse antibodies were used to visualize the bands on the immunoblotting. The membranes were analyzed by infrared imaging system and the signal intensities determined with imaging software (LI-COR) and exported to Excel. The following antibodies were used for immunoblotting studies: POLA1 (polyclonal, Santa Cruz, sc-5921; polyclonal, Sigma HPA002947; polyclonal, Bethyl Laboratories, A302–850A; polyclonal, Bethyl Laboratories, A302-851A), β-Actin (clone AC-15, Sigma, A5441), pTBK1 (clone D52C2, Cell signaling, 5483P),TBK1 (clone D1B4, Cell signaling, 3504S), pIKKε (clone D1B7, Cell signaling, 8766S), IKKε (clone D20G4, Cell signaling, 2905S), IκB-α Upstate, 06–494), p84 (clone 5E10, Genetex, GTX70220), p-Ser468 RelA (polyclonal, Cell signaling, 3039S), p-Ser536 RelA (polyclonal, Cell signaling, 3031), RelA (polyclonal, Santa Cruz, sc-372), p-Ser176/Ser177 IKK1/2 (clone C84E11, Cell signaling, 2078P), IKK2 (clone F18-1875, BD Biosciences, 551920), HA (clone 16B12, Covance, MMS101R), Lamin A/C (polyclonal, Cell signaling, 2032S), GAPDH (clone GT239, Genetex, GTX627408), GCN5 (polyclonal, Santa Cruz, sc-20698), IRF3 (clone D83B9, Cell signaling, 4302S), p-Ser396 IRF3 (clone 4D4G, Cell signaling, 4947S).

Picogreen® beads assay

The cellular cytosolic fraction were obtained as previously described [50]. Cytoplasmic fractions were precleared with 10 μL of Protein-G agarose slurry for 30 minutes at 4°C, and incubated overnight with 10 μg of control IgG, RNA:DNA antibody (clone S9.6, Kerafast, ENH001), or 10 μg of dsDNA antibody (clone AE-2, Millipore, MAB1293). To control for immunoprecipitation efficiency, a positive control antibody was co-incubated in each reaction (2 μg of RelA antibody, sc-372) along with 20 μl of Protein-G agarose slurry. After incubation, beads were washed 3 times with Triton X-100 buffer (50 mM Tris-HCL, pH 8, 100 mM NaCl, 1% Triton X-100). If required, selected samples were incubated with 0.25 μg/μl RNase A (Invitrogen) or 50 U/mL DNAse I (Invitrogen) at 37°C for 30 minutes. About 25% of the bead material was stained with Picogreen® (1:1000 dilution in PBS), and captured by fluorescence microscope (20X, Deltavision deconvolution microscopes) or confocal microscope (20X, LSM-710 laser scanning confocal microscope). The rest of the beads were boiled with 25 μl of NuPage LDS Sample Buffer (Life Technology) and analyzed by immunoblotting. Quantification of fluorescence images was performed using ImageJ.

Author Manuscript Author Manuscript Author Manuscript Author Manuscript

Cell treatment with RNA:DNA complexes

Extraction of native RNA:DNA complexes was performed according to the following method. The cellular cytosolic fraction were obtained as previously described[50]. A cytosolic fraction extracted from 15–20×10^6 cells were precleared with 10 μl of Protein-G agarose slurry for 30 minutes at 4°C, and incubated overnight with 10 μg of RNA:DNA antibody (clone S9.6, Kerafast, ENH001), anti-POLA1 antibody (polyclonal, Santa Cruz, sc-5921) or non-specific IgG as control, together with 20 μL of Protein-G agarose slurry. Following 3 washing steps with Triton X-100 buffer (50 mM Tris-HCL, pH 8, 100 mM NaCl, 1% Triton X-100), beads were incubated with 50 μL of TE buffer (10 mM Tris-HCl, pH 7.5, 1mM EDTA) supplemented with 2% SDS for 10 minutes at 75°C. SDS concentration was diluted down by adding 450 μl of hot water, and heated 10 minutes at 75°C. Samples were slowly cooled down to room temperature. The supernatants were collected and eluted nucleic acids were precipitated using a standard phenol/ethanol precipitation procedure. The pellet was reconstituted in 50 μL of TE and analyzed by on chip capillary electrophoresis (Agilent 21000 Bioanalyzer) or by conventional agarose gel electrophoresis. RNA:DNA was stored at −20°C, and transfected into the cells (1μg/mL, 16 hours) using LyoVec (Invivogen) as the transfection reagent following the original protocol. Alternatively, we also utilized synthetic RNA:DNA duplexes which consisted of an RNA:DNA forward chimeric primer: 5'-r[CGGCGGGCAG]d[CCTGGATGGG AATTCCCATCCAGGGAT] - 3', and complemented with a DNA primer: 5'-d[ATCCCTGGAT GGGAATTCCCATCCAGGCTGCCCGCCG]-3' (Sigma).

On-chip DNA and RNA capillary electrophoresis

The RNA:DNA samples were prepared as described above. The samples were quantified using Quant-iT™ PicoGreen® dsDNA Assay Kit (ThermoFisher Scientific, Grand Island, NY) according to manufacturer's protocol. The samples were analyzed on 2100 Bioanalyzer (Agilent Technologies, Santa Clara, CA) using High Sensitivity DNA Analysis or RNA Analysis kits, and further quantified against internal standards as per the instruction manual.

Statistical analysis

Statistical comparisons between mean values were performed using one-tailed, unpaired, homoscedastic, Student's *t*-test.

Supplementary Material

Refer to Web version on PubMed Central for supplementary material.

Acknowledgments

We are grateful to the patients and their families for their participation in this research project, and in particular, to the XLPDR International Association for their unwavering support for the study of this disease. We want to also thank the following individuals: Tommy Hyatt for his technical assistance with allelic discrimination assays; Yuri Pavlov (University of Nebraska), Lienhard Schmitz (Justus-Liebig-University, Germany), Jerry Shay (UT Southwestern), and Massimo Attanasio (UT Southwestern) for providing key reagents; and Helen Hobbs, Jonathan Cohen, and Zhijian (James) Chen for insightful comments and suggestions. This work was supported by NIH through the following grants: R01DK073639 (Ez.B.), R56AI113274 (Ez.B. and A.R.Z.), UL1TR001105 (J.J.R.), T32AI005284 (V.P.), R01AI098569 (N.Y.), and P30CA142543 (UT Southwestern Live Cell Imaging Facility).

Author Manuscript Author Manuscript Author Manuscript Author Manuscript

Additional support was provided by the Children's Medical Center Foundation (A.R.Z.) and the National Natural Science Foundation of China (grant 81271744 to Y.Y.).

References

1. Sancho-Shimizu V, et al. Herpes simplex encephalitis in children with autosomal recessive and dominant TRIF deficiency. J Clin Invest. 2011; 121:4889–4902. [PubMed: 22105173]
2. Hambleton S, et al. STAT2 deficiency and susceptibility to viral illness in humans. Proc Natl Acad Sci U S A. 2013; 110:3053–3058. [PubMed: 23391734]
3. Casrouge A, et al. Herpes simplex virus encephalitis in human UNC-93B deficiency. Science. 2006; 314:308–312. [PubMed: 16973841]
4. Yang YG, Lindahl T, Barnes DE. Trex1 exonuclease degrades ssDNA to prevent chronic checkpoint activation and autoimmune disease. Cell. 2007; 131:873–886. [PubMed: 18045533]
5. Mannion NM, et al. The RNA-editing enzyme ADAR1 controls innate immune responses to RNA. Cell reports. 2014; 9:1482–1494. [PubMed: 25456137]
6. Crow YJ, Manel N. Aicardi-Goutieres syndrome and the type I interferonopathies. Nat Rev Immunol. 2015; 15:429–440. [PubMed: 26052098]
7. Crow YJ, et al. Characterization of human disease phenotypes associated with mutations in TREX1, RNASEH2A, RNASEH2B, RNASEH2C, SAMHD1, ADAR, and IFIH1. Am J Med Genet A. 2015; 167A:296–312. [PubMed: 25604658]
8. Reijns MA, Jackson AP. Ribonuclease H2 in health and disease. Biochemical Society transactions. 2014; 42:717–725. [PubMed: 25109948]
9. Gunther C, et al. Defective removal of ribonucleotides from DNA promotes systemic autoimmunity. J Clin Invest. 2015; 125:413–424. [PubMed: 25500883]
10. Partington MW, Marriott PJ, Prentice RS, Cavaglia A, Simpson NE. Familial cutaneous amyloidosis with systemic manifestations in males. Am J Med Genet. 1981; 10:65–75. [PubMed: 6794369]
11. Partington MW, Prentice RS. X-linked cutaneous amyloidosis: further clinical and pathological observations. Am J Med Genet. 1989; 32:115–119. [PubMed: 2705473]
12. Ades LC, Rogers M, Sillence DO. An X-linked reticulate pigmentary disorder with systemic manifestations: report of a second family. Pediatr Dermatol. 1993; 10:344–351. [PubMed: 8302737]
13. Anderson RC, Zinn AR, Kim J, Carder KR. X-linked reticulate pigmentary disorder with systemic manifestations: report of a third family and literature review. Pediatr Dermatol. 2005; 22:122–126. [PubMed: 15804299]
14. Fernandez-Guarino M, et al. X-linked reticulate pigmentary disorder: report of a new family. European journal of dermatology : EJD. 2008; 18:102–103. [PubMed: 18086616]
15. Pezzani L, Brena M, Callea M, Colombi M, Tadini G. X-linked reticulate pigmentary disorder with systemic manifestations: a new family and review of the literature. Am J Med Genet A. 2013; 161:1414–1420. [PubMed: 23613254]
16. Kim BS, Seo SH, Jung HD, Kwon KS, Kim MB. X-Linked reticulate pigmentary disorder in a female patient. International journal of dermatology. 2010; 49:421–425. [PubMed: 20465698]
17. Megarbane H, et al. X-linked reticulate pigmentary layer. Report of a new patient and demonstration of a skewed X-inactivation. Genet Couns. 2005; 16:85–89. [PubMed: 15844784]
18. Fraile G, Norman F, Reguero ME, Defargues V, Redondo C. Cryptogenic multifocal ulcerous stenosing enteritis (CMUSE) in a man with a diagnosis of X-linked reticulate pigmentary disorder (PDR). Scand J Gastroenterol. 2008; 43:506–510. [PubMed: 18365917]
19. Picard C, Casanova JL, Puel A. Infectious diseases in patients with IRAK-4, MyD88, NEMO, or IκBα deficiency. Clin Microbiol Rev. 2011; 24:490–497. [PubMed: 21734245]
20. Jaeckle Santos LJ, et al. Refined mapping of X-linked reticulate pigmentary disorder and sequencing of candidate genes. Hum Genet. 2008; 123:469–476. [PubMed: 18404279]
21. Foley SB, et al. Use of Whole Genome Sequencing for Diagnosis and Discovery in the Cancer Genetics Clinic. EBioMedicine. 2015; 2:74–81. [PubMed: 26023681]

Author Manuscript Author Manuscript Author Manuscript Author Manuscript

22. O'Donnell M, Langston L, Stillman B. Principles and concepts of DNA replication in bacteria, archaea, and eukarya. Cold Spring Harb Perspect Biol. 2013; 5
23. Dong Q, Copeland WC, Wang TS. Mutational studies of human DNA polymerase α. Identification of residues critical for deoxynucleotide binding and misinsertion fidelity of DNA synthesis. J Biol Chem. 1993; 268:24163–24174. [PubMed: 8226963]
24. Kunkel TA, Burgers PM. Dividing the workload at a eukaryotic replication fork. Trends Cell Biol. 2008; 18:521–527. [PubMed: 18824354]
25. Murakami Y, Yasuda H, Miyazawa H, Hanaoka F, Yamada M. Characterization of a temperature-sensitive mutant of mouse FM3A cells defective in DNA replication. Proc Natl Acad Sci U S A. 1985; 82:1761–1765. [PubMed: 3856858]
26. Victor RG, et al. The Dallas Heart Study: a population-based probability sample for the multidisciplinary study of ethnic differences in cardiovascular health. Am J Cardiol. 2004; 93:1473–1480. [PubMed: 15194016]
27. Petrovski S, Wang Q, Heinzen EL, Allen AS, Goldstein DB. Genic intolerance to functional variation and the interpretation of personal genomes. PLoS Genet. 2013; 9:e1003709. [PubMed: 23990802]
28. Huff CD, et al. Maximum-likelihood estimation of recent shared ancestry (ERSA). Genome research. 2011; 21:768–774. [PubMed: 21324875]
29. Browning SR, Browning BL. High-resolution detection of identity by descent in unrelated individuals. Am J Hum Genet. 2010; 86:526–539. [PubMed: 20303063]
30. Dogan RI, Getoor L, Wilbur WJ, Mount SM. SplicePort--an interactive splice-site analysis tool. Nucleic Acids Res. 2007; 35:W285–291. [PubMed: 17576680]
31. Kishore S, Khanna A, Stamm S. Rapid generation of splicing reporters with pSpliceExpress. Gene. 2008; 427:104–110. [PubMed: 18930792]
32. Bogunovic D, et al. Mycobacterial disease and impaired IFN-γ immunity in humans with inherited ISG15 deficiency. Science. 2012; 337:1684–1688. [PubMed: 22859821]
33. Zhang X, et al. Human intracellular ISG15 prevents interferon-α/β over-amplification and auto-inflammation. Nature. 2015; 517:89–93. [PubMed: 25307056]
34. Puel A, et al. Chronic mucocutaneous candidiasis in humans with inborn errors of interleukin-17 immunity. Science. 2011; 332:65–68. [PubMed: 21350122]
35. Lee MS, Kim YJ. Signaling pathways downstream of pattern-recognition receptors and their cross talk. Annu Rev Biochem. 2007; 76:447–480. [PubMed: 17328678]
36. Hayden MS, Ghosh S. NF-κB, the first quarter-century: remarkable progress and outstanding questions. Genes Dev. 2012; 26:203–234. [PubMed: 22302935]
37. Ysebrant de Lendonck L, et al. Interferon regulatory factor 3 controls interleukin-17 expression in CD8 T lymphocytes. Proc Natl Acad Sci U S A. 2013; 110:E3189–3197. [PubMed: 23918362]
38. Asplund A, Edqvist PH, Schwenk JM, Ponten F. Antibodies for profiling the human proteome-The Human Protein Atlas as a resource for cancer research. Proteomics. 2012; 12:2067–2077. [PubMed: 22623277]
39. Brown M, Bollum FJ, Chang LM. Intracellular localization of DNA polymerase α. Proc Natl Acad Sci U S A. 1981; 78:3049–3052. [PubMed: 7019918]
40. Mankan AK, et al. Cytosolic RNA:DNA hybrids activate the cGAS-STING axis. EMBO J. 2014; 33:2937–2946. [PubMed: 25425575]
41. Dobbs N, et al. STING Activation by Translocation from the ER Is Associated with Infection and Autoinflammatory Disease. Cell Host Microbe. 2015; 18:157–168. [PubMed: 26235147]
42. Neitzel H. A routine method for the establishment of permanent growing lymphoblastoid cell lines. Hum Genet. 1986; 73:320–326. [PubMed: 3017841]
43. Uphoff CC, Denkmann SA, Drexler HG. Treatment of mycoplasma contamination in cell cultures with Plasmocin. Journal of biomedicine & biotechnology. 2012; 2012:267678. [PubMed: 23091342]
44. Duckett CS, Gedrich RW, Gilfillan MC, Thompson CB. Induction of nuclear factor κB by the CD30 receptor is mediated by TRAF1 and TRAF2. Mol Cell Biol. 1997; 17:1535–1542. [PubMed: 9032281]

Author Manuscript Author Manuscript Author Manuscript Author Manuscript

45. Lois C, Hong EJ, Pease S, Brown EJ, Baltimore D. Germline transmission and tissue-specific expression of transgenes delivered by lentiviral vectors. Science. 2002; 295:868–872. [PubMed: 11786607]

46. Starokadomskyy P, et al. CCDC22 deficiency in humans blunts activation of proinflammatory NF-κB signaling. J Clin Invest. 2013; 123:2244–2256. [PubMed: 23563313]

47. Dozmorov I, Lefkovits I. Internal standard-based analysis of microarray data. Part 1: analysis of differential gene expressions. Nucleic Acids Res. 2009; 37:6323–6339. [PubMed: 19720734]

48. Dozmorov MG, Guthridge JM, Hurst RE, Dozmorov IM. A comprehensive and universal method for assessing the performance of differential gene expression analyses. PLoS One. 2010; 5

49. Li QZ, et al. Protein array autoantibody profiles for insights into systemic lupus erythematosus and incomplete lupus syndromes. Clinical and experimental immunology. 2007; 147:60–70. [PubMed: 17177964]

50. Li H, Starokadomskyy P, Burstein E. Methodology to study NF-κB/RelA ubiquitination in vivo. Methods Mol Biol. 2015; 1280:371–381. [PubMed: 25736761]

Author Manuscript Author Manuscript Author Manuscript Author Manuscript

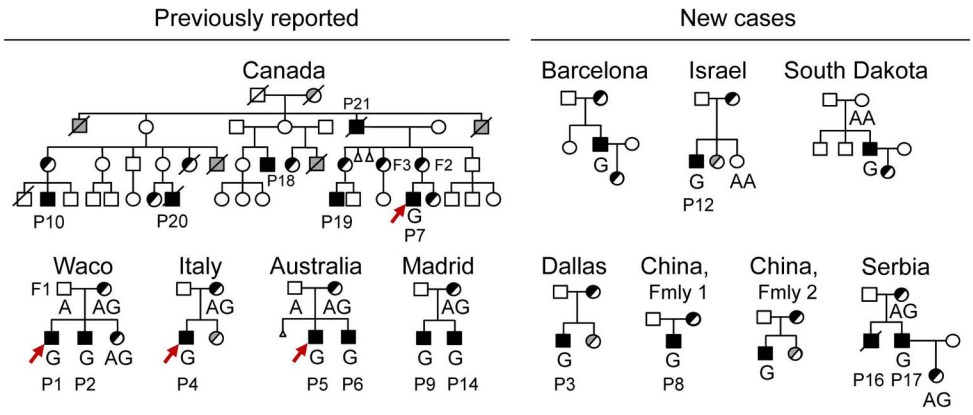

Figure 1. Whole genome sequencing identifies a recurrent intronic mutation as the cause of XLPDR

Whole genome sequencing followed by targeted genotyping was performed. Pedigrees of eleven families with XLPDR analyzed here are shown, including seven new cases (place of origin is noted). Probands and relatives examined elsewhere in the paper are indicated (P1 to P21, and F1 to F3). Red arrows depict the probands whose DNA was analyzed by whole genome sequencing. Possible cases or carriers are indicated in gray. Results of genotyping for the intronic mutation in *POLA1* are noted (A, wild-type allele; G, XLPDR-associated allele).

Author Manuscript Author Manuscript Author Manuscript Author Manuscript

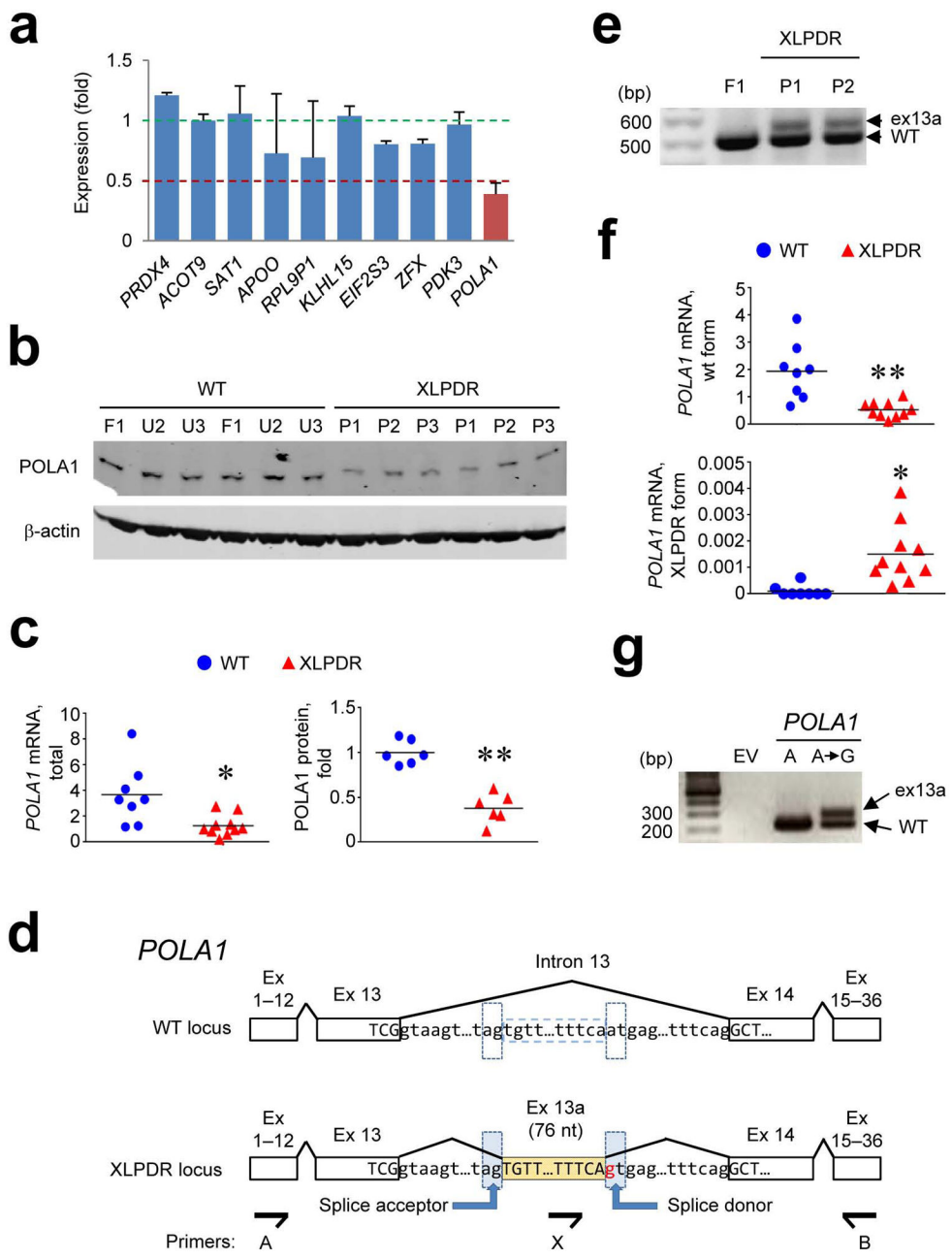

Figure 2. XLPDR is due to an intronic mutation that disrupts *POLA1* expression

(**a**) RNA-seq quantification of gene expression across the XLPDR linkage interval in XLPDR-derived dermal fibroblasts (P1, P2, P3) was normalized against four normal fibroblast cell lines (F1, and three lines from unrelated males, U1, U2, U3). Only genes with detectable expression are displayed. (**b**) Immunoblotting determination of POLA1 protein expression in dermal fibroblasts from unaffected control lines and XLPDR-derived cells. (**c**) Quantitative RT-PCR (qRT-PCR) for *POLA1* mRNA (left panel) in multiple independent samples from dermal fibroblasts from unaffected individuals (8 samples, 4 cell lines) and XLPDR patients (10 samples, 2 cell lines). *POLA1* mRNA level is normalized to *ACTB*

Author Manuscript Author Manuscript Author Manuscript Author Manuscript

($\times 10^{-3}$). In addition, quantification of POLA1 protein levels shown in (b) are similarly presented (right panel). (**d**) Schematic representation of the mutation in intron 13 of the *POLA1* gene. The location of primers used for RT-PCR are noted. Ex – exon. (**e**) RT-PCR using primers A and B (see d) and RNA from XLPDR-derived fibroblasts and a control line. The amplified products were separated by agarose gel electrophoresis and visualized with ethidium bromide. (**f**) qRT-PCR using transcript-specific primers for wild-type and misspliced forms of *POLA1* mRNA from dermal fibroblasts from unaffected individuals (8 samples, 4 cell lines) and XLPDR patients (10 samples, 2 cell lines) was performed. (**g**) Exon trapping analysis in cells transfected with pSpliceExpress plasmids containing empty vector (EV), the wild type *POLA1* intron 13 (A), or the intron bearing the XLPDR mutation (A→G). RT-PCR amplified products were analyzed by agarose gel electrophoresis and visualized with ethidium bromide staining. *p<0.005, **p<0.001 (unpaired Student's *t*-test). Data are pooled from 3 independent experiments (**a**), or representative from 2 (**e,f,g**) or 4 (**b,e**) independent experiments (mean and s.e.m.(**a**) or mean and individual sample values (**c,f**)).

Author Manuscript Author Manuscript Author Manuscript Author Manuscript

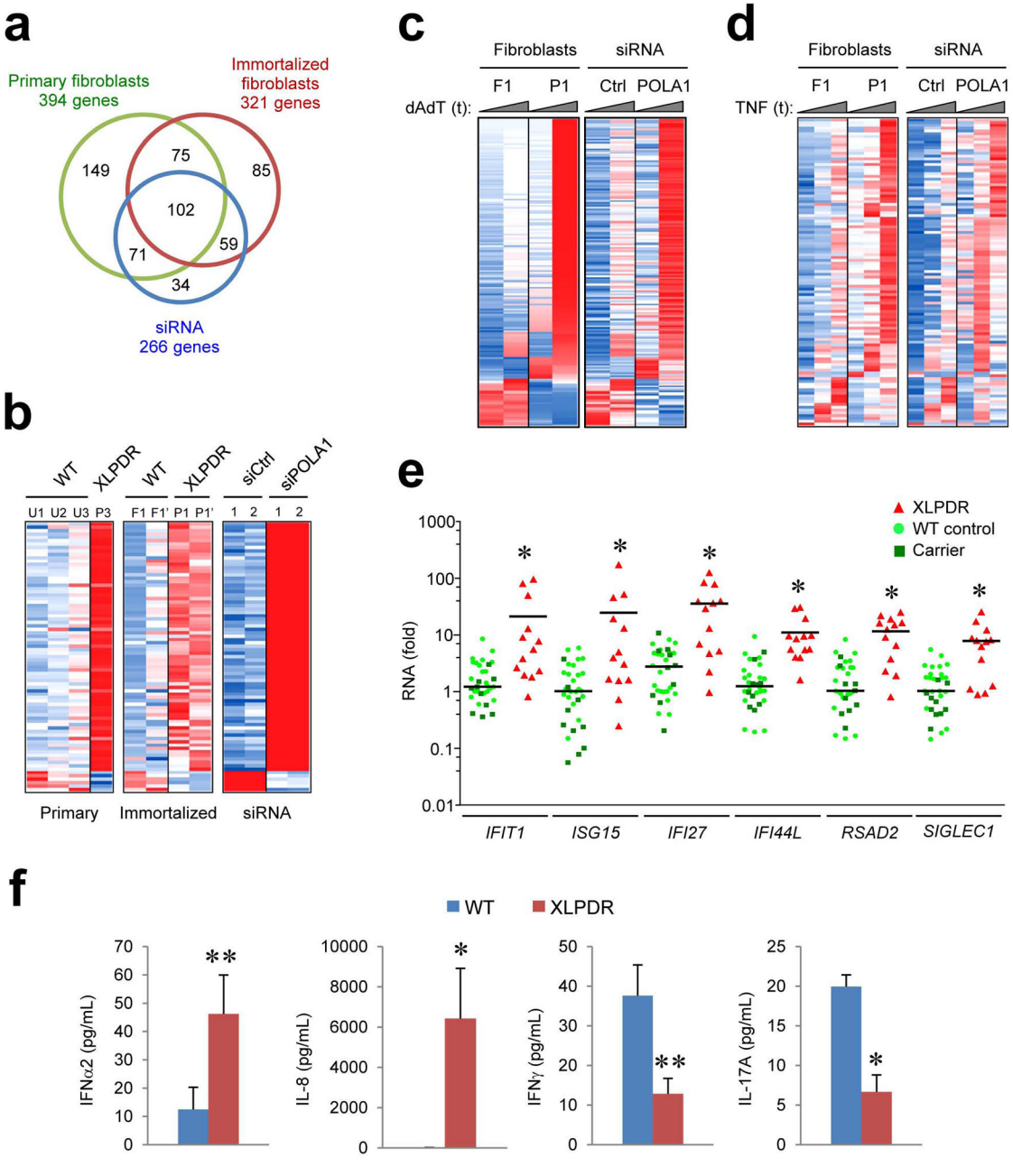

Figure 3. *POLA1* deficiency results in type-I interferon activation

(**a**) Venn diagram illustrating the transcriptomic changes noted by RNA-seq as a result of *POLA1* deficiency in three cellular models: primary fibroblasts, immortalized fibroblasts, and normal fibroblasts after siRNA for POLA1. (**b**) Heatmap display of RNA-seq data showing concurrent alterations in basal gene expression in primary and immortalized XLPDR fibroblasts, as well as normal fibroblasts after POLA1 silencing. The siRNA experiment represents two iterations using different siRNA duplexes (1 and 2). Blue indicates downregulation and red indicates upregulation of the corresponding gene. (**c**) Similar to (b), heatmap display of RNA-seq data showing genes with concurrent alterations

Author Manuscript Author Manuscript Author Manuscript Author Manuscript

in immortalized XLPDR fibroblasts (left panel) and POLA1 silencing (right panel) after poly(dA:dT) stimulation (16h). (**d**) Similar to (c), but in this experiment cells were stimulated with TNF (2h or 12h). (**e**) qRT-PCR analysis of interferon-stimulated genes (ISGs) in whole blood-derived RNA from XLPDR probands (n=5), unaffected 'travel' controls (n=9) and heterozygous carriers (n=5). All samples were taken at least in duplicate. Transcript abundance is displayed as the fold compared to the same reference control sample. (**f**) Multiplex bead analysis of cytokine plasma levels in XLPDR probands (n=3) and healthy individuals (n=4). *p<0.01, **p<0.05 (unpaired Student's *t*-test). Data are pooled from 3 independent experiments (**a**), or obtained by comparison of 2 (**c,d**) or 4 (**b**) independent models of XLPDR, (**e, f**) were performed one time (mean and individual sample values (**e**) or mean and s.e.m.(**f**)).

Author Manuscript Author Manuscript Author Manuscript Author Manuscript

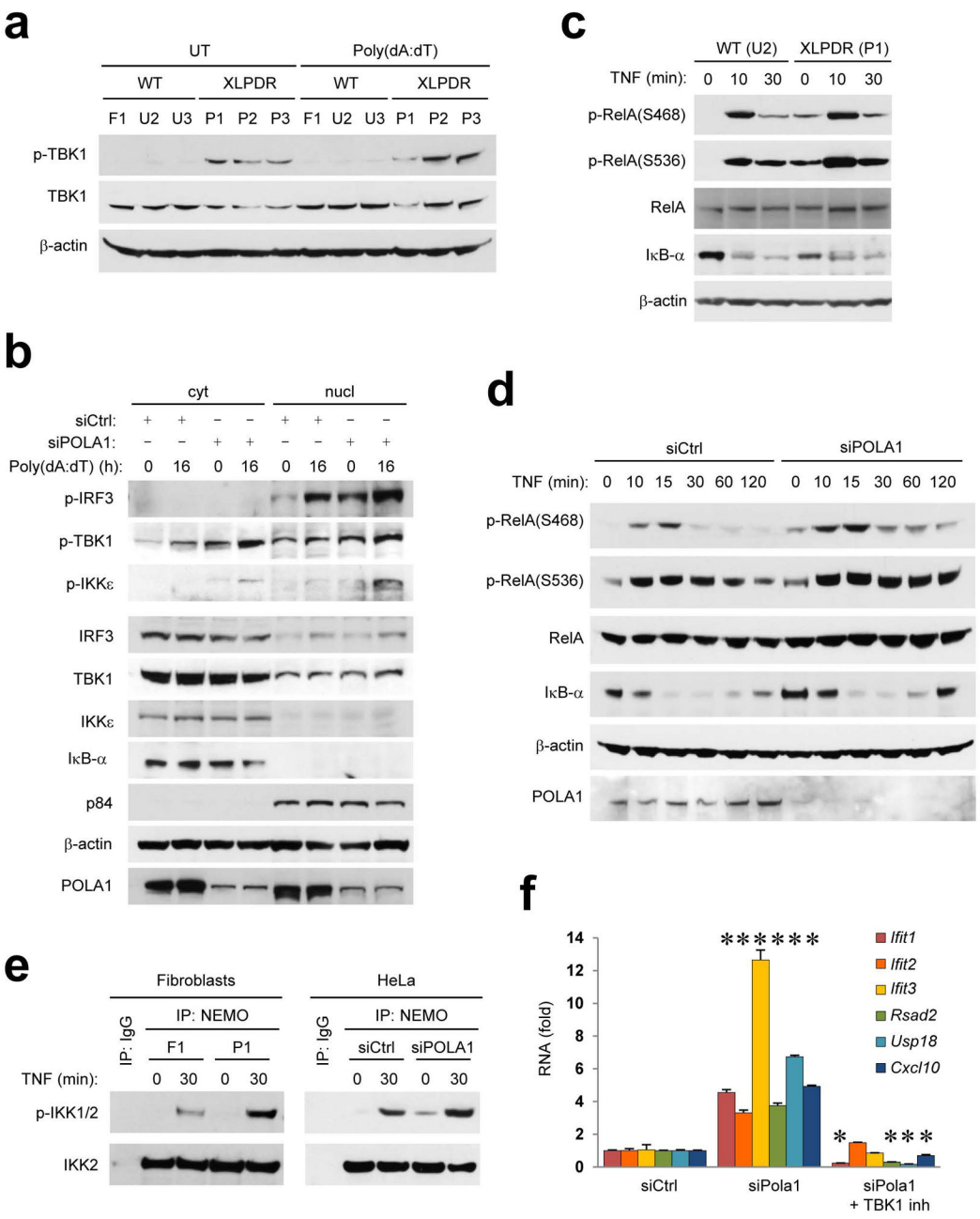

Figure 4. *POLA1* deficiency leads to excessive activation of IRF and NF-κB pathways

(**a**) Immunoblot analysis of total and phosphorylated (p-) TBK1, and β-actin (loading control throughout) in lysates of wild-type and XLPDR fibroblasts left untreated (UT) or treated with poly(dA:dT) (16 h). (**b**) Immunoblot analysis of TBK1, IKKε and IRF3 (total and phosphorylated forms) in cytosolic (cyt) and nuclear (nucl) fractions of HeLa cells transfected with siRNA. When indicated, cells were treated with poly(dA:dT) as before. IκB-α and p84 serve as markers for the cytosolic and nuclear fractions, respectively. (**c**) Immunoblot analysis of total and p-RelA (on either S468 or S536), and IκB-α, in control and XLPDR-derived fibroblasts. When indicated, cells were treated with TNF. (**d**)

Author Manuscript Author Manuscript Author Manuscript Author Manuscript

Immunoblot analysis of RelA (total and phosphorylated forms) and IκB-α, in HeLa cells after POLA1 siRNA. When indicated, cells were treated with TNF. **(e)** Immunoblot analysis for the active form of the IKK complex (p-IKK1/2) after immunoprecipitation of the complex with a NEMO antibody. Control and XLPDR-derived fibroblasts were examined (left), as well as HeLa cells after POLA1 siRNA (right). When indicated, cells were treated with TNF. (**f**) qRT-PCR analysis of ISGs in wild-type (WT) mouse embryo fibroblasts (MEFs) after treatment with the TBK1 inhibitor (inh) BX795. *$p<0.05$ when compared to the control group (unpaired Student's *t* test). Data are representative of 2 (**a**), 3(**c,e,f**) or 4 (**b,d**) independent experiments (mean and s.e.m.(**f**)).

Author Manuscript Author Manuscript Author Manuscript Author Manuscript

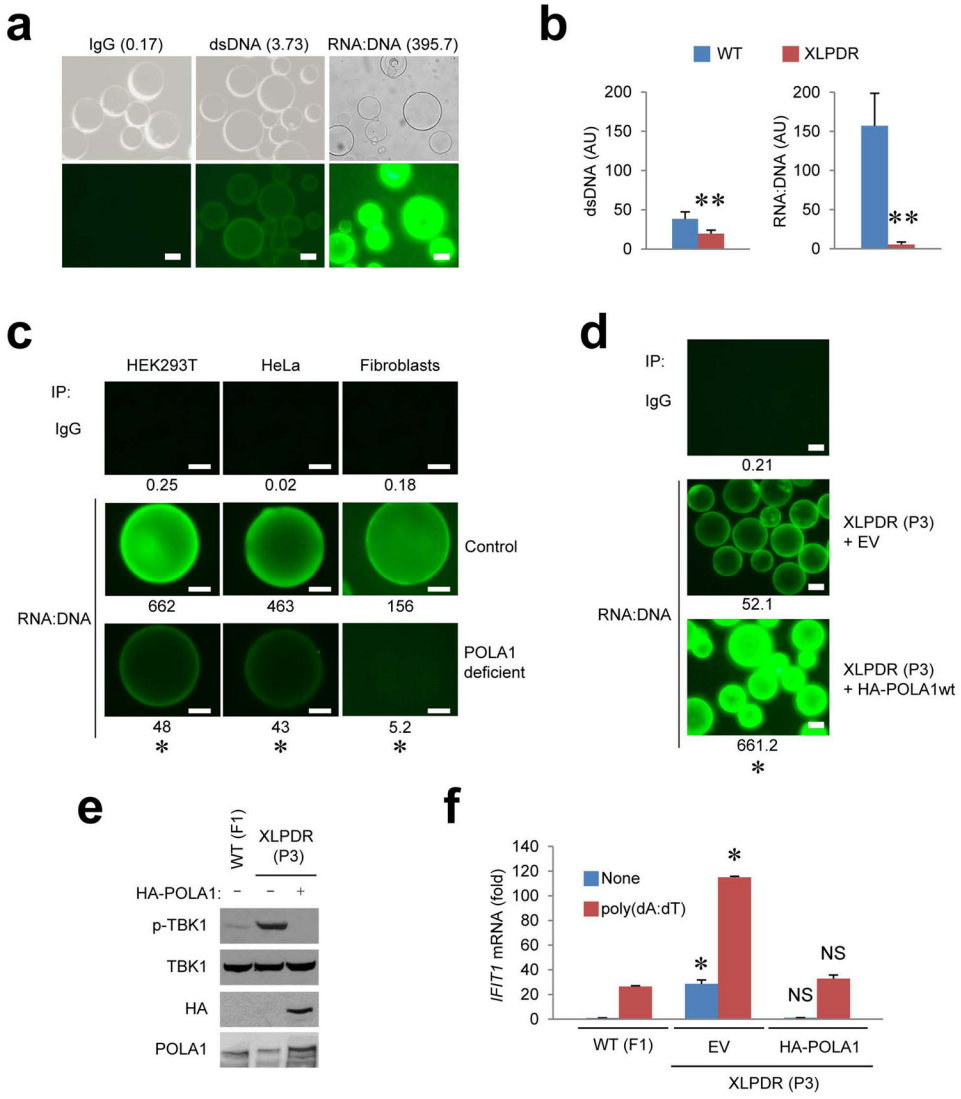

Figure 5. *POLA1* deficiency is associated with reduced cytosolic RNA:DNA levels

(**a**) Immunoprecipitation of dsDNA and RNA:DNA from cytosolic fractions of HEK293T cells using the corresponding antibodies and Protein-G agarose beads. Beads were stained with Picogreen® and visualized by fluorescence microscopy. Nucleic acid recovery was quantified by image analysis (ImageJ). Mean relative fluorescence levels are indicated in parantheses. (**b**) As in (a), dsDNA or RNA:DNA were quantified in control or XLPDR-derived fibroblasts. (**c**) RNA:DNA was quantified in a similar manner in three models of *POLA1* deficiency: HEK293T and HeLa after POLA1 silencing (compared to control siRNA), and XLPDR-derived dermal fibroblasts (compared to control cells). Representative images are shown and relative fluorescence levels are indicated. (**d**) Cytosolic RNA:DNA content was quantified in XLPDR-derived fibroblasts stably transduced with a lentivirus encoding HA-tagged wild-type POLA1 (HA-POLA1wt) or EV. Representative images and relative fluorescence levels are indicated. (**e**) Immunoblot analysis of total and p-TBK1, and total and HA-tagged POLA1 expression in XLPDR fibroblast stably expressing HA-POLA1wt or EV (as in d). (**f**) qRT-PCR analysis of *IFIT1* mRNA expression in the same

Author Manuscript Author Manuscript Author Manuscript Author Manuscript

cells depicted in (d); when indicated, the cells were treated with poly(dA:dT) for 16h. Scale bars are 20 μm. *p≤0.05, **p≤0.01, NS – not significant (unpaired Student's *t*-test). In (**f**) all comparisons are made against the corresponding WT conditions. Data are representative of 1 (**d,e**), 2 (**a,b,f**), or 4 (**c**) independent experiments (mean (**a,c,d**) and mean and s.e.m.(**b,f**)).

Author Manuscript Author Manuscript Author Manuscript Author Manuscript

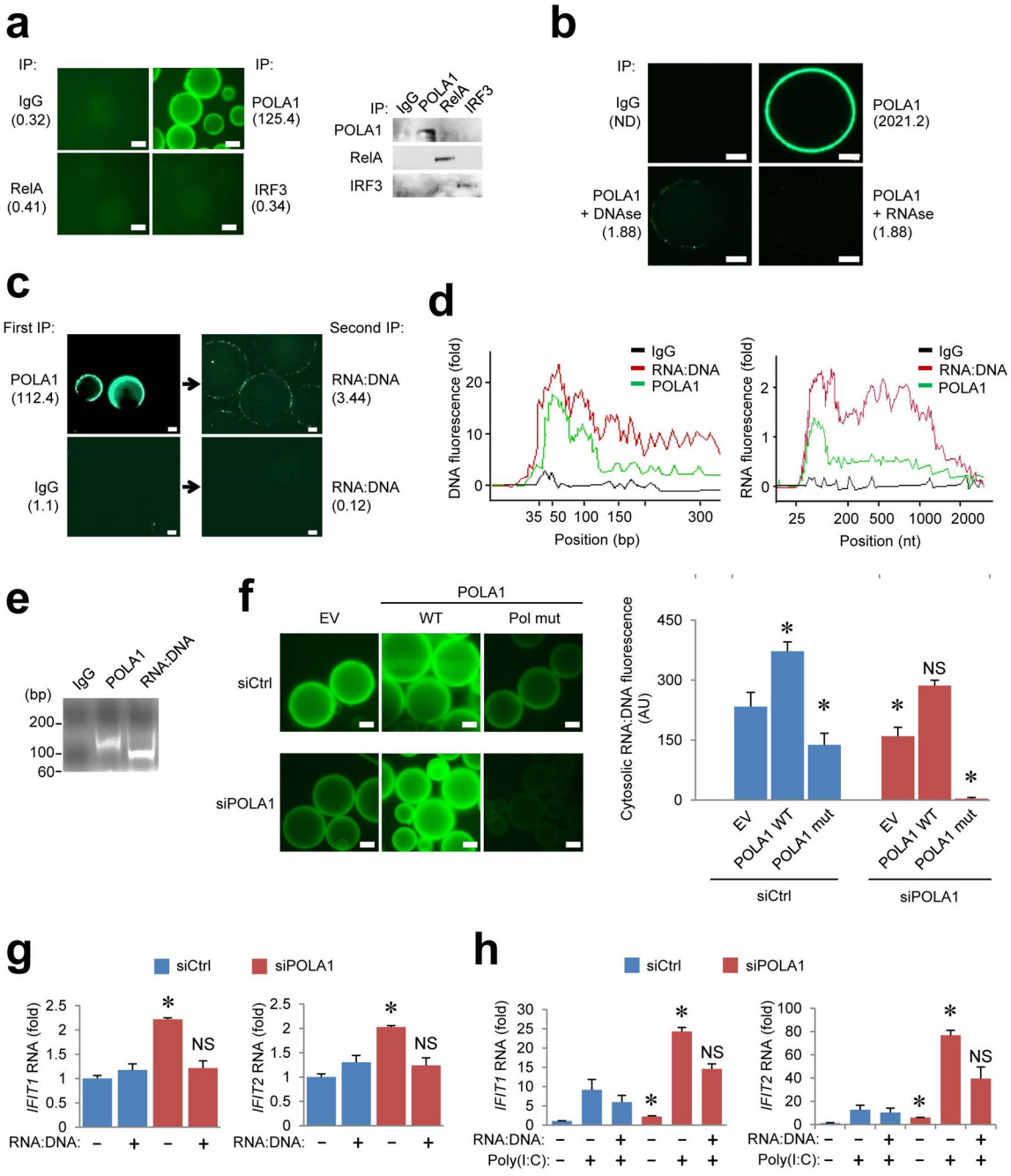

Figure 6. Cytosolic RNA:DNA attenuates IRF activation

(**a**) Immunoprecipitation of the indicated proteins from the cytosolic fraction of HEK293T was followed by Picogreen® staining and fluorescence quantification. Represetative images and fluorescence intensities (in parantheses) are presented (left panels); immunoblotting for the precipitated proteins is also shown (right panels). (**b**) POLA1 was immunoprecipitated as in (a), and the recovered beads were treated with RNaseA or DNAseI prior to Picogreen® staining. Fluorescence levels are indicated in parentheses. (**c**) Cytosolic POLA1 immunoprecipitation (left) was followed by nucleic acid elution and re-immunoprecipitated

Author Manuscript Author Manuscript Author Manuscript Author Manuscript

by RNA:DNA antibody (right). Beads were stained with Picogreen® and visualized by confocal microscopy. Relative fluorescence levels are indicated in parantheses. (**d**) Nucleic acids immunoprecipitated from cytosolic fractions, either directly by an RNA:DNA antibody or using a POLA1 antibody, were eluted as in (c) and analyzed by on-chip DNA or RNA capillary electrophoresis. (**e**) Similar to (d), nucleic acids were separated by agarose gel electrophoresis and visualized by ethidium bromide staining. (**f**) Cytosolic RNA:DNA content was quantified by immunoprecipitation and bead staining in HEK293T cells transfected as indicated. Representative images are shown (left) and fluorescence values are plotted (right). (**g**) qRT-PCR analysis of *IFIT1* and *IFIT2* mRNA expression in HeLa cells transfected with the indicated siRNA and also transfected with native cytosolic RNA:DNA extracted from HEK293T cells. (**h**) Similar to (g), but using synthetic RNA:DNA duplexes that were transfected into HeLa cells; when indicated, cells were stimulated with poly(I:C) (for 8h). Scale bars are 20 μm. *$p<0.05$ (unpaired Student's *t* test). In (**f**) all values were compared to control (siCtrl, EV) conditions. In (**g,h**), the siPOLA1 values were compared to the corresponding conditions in the siCtrl group. Data are from 1 experiment (**c**), or representative of 2 (**b,f,e**), 3 (**h**) or 4 (**a,g**) independent experiments (mean (**a**) and mean and s.e.m.(**f,g,h**)).

Author Manuscript Author Manuscript Author Manuscript Author Manuscript

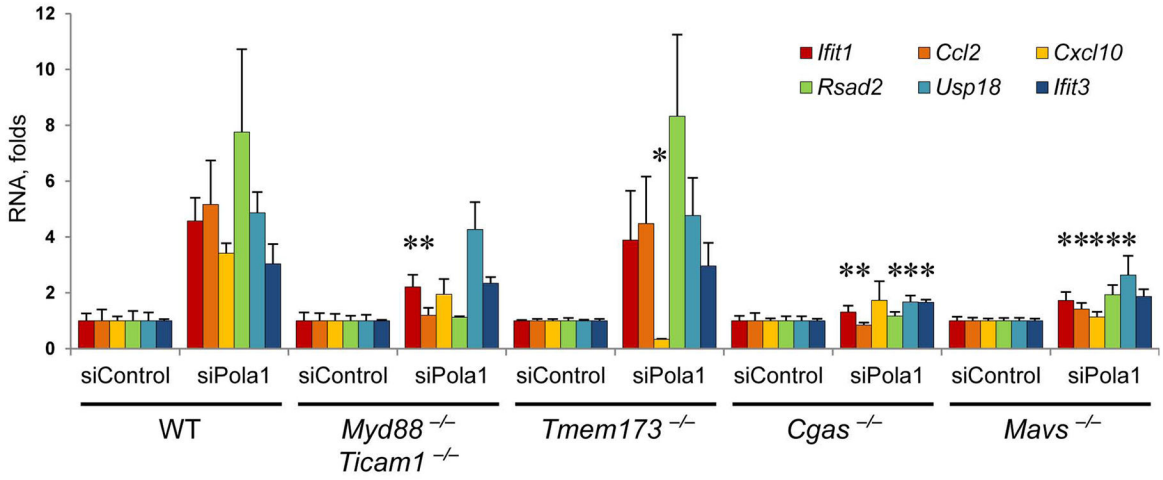

Figure 7. Cytosolic RNA:DNA generation by POLA1 modulates nucleic acid sensor pathways

qRT-PCR quantification of six ISGs after siRNA for Pola1 in MEFs from WT embryos or specific knockout strains, as indicated. *p<0.05 when compared to the corresponding conditions in WT MEFs (unpaired Student's *t* test). Data are pooled from 4 independent experiments (mean and s.e.m.).

Author Manuscript

Author Manuscript

Author Manuscript

Author Manuscript

TABLE

Bioinformatic analysis of the gene alterations noted in Fig. 3b using Ingenuity Pathway Analysis, focusing on shared canonical pathways and upstream regulators.

Ingenuity Canonical Pathways	**z-score**
Interferon Signaling	2.646
Role of Pattern Recognition Receptors in Recognition of Bacteria and Viruses	2.000
Upstream Regulator	**p-value**
IRF7	5.25E-53
IRF1	8.66E-38
IRF3	8.04E-35
STAT1	8.64E-33
TRIM24	9.87E-31
STAT2	4.31E-28
NKX2-3	2.07E-28
CNOT7	2.63E-27
IRF5	1.07E-25
IRF9	8.25E-18
NLRC5	1.39E-13
BRCA1	6.28E-11
RELA	3.33E-09